MagMonitor: Vehicle Speed Estimation and Vehicle Classification Through A Magnetic Sensor

Yimeng Feng, *Graduate Student Member, IEEE*, Guoqiang Mao, *Fellow, IEEE*, Bo Cheng, *Member, IEEE*, Changle Li, *Senior Member, IEEE*, Yilong Hui, *Member, IEEE*, Zhigang Xu, *Member, IEEE*, and Junliang Chen, *Senior Member, IEEE*

***Abstract*— Internet of Things (IoT) is playing an increasingly important role in Intelligent Transportation Systems (ITS) for real-time sensing and communication. In ITS, vehicle types, volume and speeds provide important information for road traffic management. However, the present methods for on-road traffic monitoring are lacking in providing cost-effective means to meet the demands. In this paper, we propose MagMonitor, a novel method for on-road traffic surveillance through a single small and easy-to-install magnetic sensor. The developed magnetic sensor system is wireless-connected, cost-effective, and environmental-friendly. First, a magnetic model of a moving vehicle is presented. The model employs multiple magnetic dipoles for modelling moving vehicle and varies depending on the on-road vehicle types. Through modelling of local magnetic field perturbations caused by moving vehicles, we extract the characteristics of magnetic waveforms for vehicle identification and speed estimation. The proposed model and estimation technique are validated with real field experimental data. Furthermore, we analyze and compare the performance of the proposed estimation technique with other speed estimation algorithms, which shows the superior accuracy of the proposed technique.**

***Index Terms*— Magnetic sensor, vehicle classification, speed estimation, traffic surveillance, signal processing.**

I. Introduction

INTELLIGENT transportation systems (ITS) developed rapidly over the last decades. The main purpose of ITS is to enhance the transportation system's safety, efficiency, and cost effectiveness [1], [2]. Traffic surveillance provides valuable traffic flow information for ITS through various kinds of traffic sensors, such as LiDar, microwave sensors and magnetic sensors [3]–[5]. The traffic surveillance information can then be used by ITS to improve traffic management [6].

The fine-grained monitoring of vehicle speed plays an important role in ITS. The U.S. National Highway Traffic Safety Administration (NHTSA) reported 37,461 traffic fatalities in 2016, 26% of which are speed-related [7]. Many traffic surveillance technologies are introduced and have been studied for traffic data collection, such as inductive loops [8], video based image processing methods [9], etc. Particularly, urban areas have many complex environments, traffic situation awareness and estimation needs accurate vehicle speed data. In this paper, we focus on the problem of accurate vehicle speed estimation using a single on-road magnetic sensor.

Recently, magnetic sensors are considered for vehicle speed estimation [10]. Current vehicle speed acquisition methods using magnetic sensors often employ more than one magnetic sensors [11], [12]. However, using two or more well separated magnetic sensors for speed estimation, requires these magnetic sensor units to be very well synchronized and their data to be communicated in real-time, which significantly increases both the energy consumption and communication overheads. Both the energy consumption and communication overhead are main considerations for small and energy-constrained Internet of Things (IoT) devices. Furthermore, the use of two or more magnetic sensor units will significantly increase the size of the IoT device, which also prohibits its easy installation and hence widespread use.

To this end, in this paper we consider a new approach, which uses a single magnetic sensor to classify vehicle types and estimate vehicle speeds. The underlying idea is to measure the local magnetic field perturbations when vehicles passing by the roadside magnetic sensor. Several challenges arise in the design of the proposed approach. First, using only one sensor to estimate the aforementioned parameters needs a thorough understanding of a metal object's magnetic characteristics. Second, accurate modelling of the local magnetic field perturbation caused by various types of vehicles is essential. Finally, the magnetic sensor readings are noisy and the environment noise needs to be considered and removed to obtain accurate estimation.

This paper presents MagMonitor, a novel real-time traffic surveillance technique that provides vehicle classification and speed estimation using a single small magnetic sensor.

Manuscript received February 19, 2020; revised June 9, 2020 and July 27, 2020; accepted September 8, 2020. This work was supported in part by the National Key Research and Development Program of China under Grant 2019YFB1600100, in part by the National Natural Science Foundation of China under Grant 61921003 and Grant 61972043, and in part by the BUPT Ph.D. Short-Term Overseas Study Project. The Associate Editor for this article was M. Zhou. *(Corresponding author: Guoqiang Mao.)*

Yimeng Feng is with the State Key Laboratory of Networking and Switching Technology, Beijing University of Posts and Telecommunications, Beijing 100088, China, and also with the School of Electrical and Data Engineering, University of Technology Sydney, Ultimo, NSW 2007, Australia (e-mail: fyimeng@bupt.edu.cn).

Guoqiang Mao is with the School of Telecommunications Engineering, Xidian University, Xi'an 710071, China (e-mail: g.mao@ieee.org).

Bo Cheng and Junliang Chen are with the State Key Laboratory of Networking and Switching Technology, Beijing University of Posts and Telecommunications, Beijing 100088, China (e-mail: chengbo@bupt.edu.cn; chjl@bupt.edu.cn).

Changle Li and Yilong Hui are with the State Key Laboratory of Integrated Services Networks, Xidian University, Xi'an 710071, China (e-mail: clli@xidian.edu.cn; ylhui@xidian.edu.cn).

Zhigang Xu is with the School of Information Engineering, Chang'an University, Xi'an 710071, China (e-mail: xuzhigang@chd.edu.cn).

Digital Object Identifier 10.1109/TITS.2020.3024652

It identifies vehicle magnetic characteristics by modelling various types of vehicles using multiple magnetic dipoles. For each type of vehicle, we estimate the speeds through their separate magnetic waveforms. A filter of raw magnetic data is employed for reducing the environmental noise, and yield an accurate magnetic output caused by moving vehicles. The magnetic sensor used in the experiment is easy to install and cost efficient to implement on road, which is also relatively environmental-friendly. Experiments are conducted in Xi'an, China to establish the effectiveness of the proposed technique.

Specifically, our key contributions are threefold:

- We propose a method of monitoring the on-road vehicle types and obtain vehicle speeds through observations on magnetic perturbations. The magnetic sensor used in the experiment is tiny, cost-effective, and wireless-connected to capture real-time traffic conditions.
- We conduct simulations on the magnetic dipole models. Combined with vehicle dynamics, we present a motion model which illustrates the local magnetic field perturbation caused by a moving vehicle and validate the results using the measured magnetic perturbations caused by moving vehicles.
- We develop signal processing technique for data processing, which provides filtered magnetic waveforms for vehicle counting and speed estimation. Road experiments are conducted to validate the effectiveness of the proposed technique.

The rest of the paper is organized as follows: Section II briefly reviews related works on real-time road surveillance. Section III describes the design of multiple magnetic models and vehicle motion characteristics. Section IV introduces the sensor model based experimental results and discussions for vehicle classification and speed estimation. Finally, Section V concludes the paper and discusses our future work.

II. Review of Related Work For Real-Time Road Surveillance

In this section, we review current methods for vehicle speed estimation, which is divided into two sub-sections. One is general methods of on-road traffic information acquisition, the other is vehicle classification and speed estimation using magnetometers.

A. General Methods of Real-Time Road Surveillance

Many techniques are used on highways or urban roads for speed estimation, such as inductive loops, vision based image processing method, and Global Positioning System (GPS) on smartphone [13].

Inductive loop detectors embedded into the road surface are considered as intrusive methods [8]. These detectors are required to be installed underneath the road surface, which results in very high installation and maintenance costs. To reduce installation and maintenance costs, vision based traffic camera systems have been adopted [9]. However, the resulting data transmission volume is large and the estimation accuracy is weather and visibility dependent. In other words, the accuracy of vision based system suffers in poor weather conditions, low illumination and visibility conditions. Radar is used to detect objects in a distance and estimate their speed [14], but it takes more time to lock on an object. Although LiDar can detect objects on the ground precisely, it is very expensive. Reference [15] developed a technique using GPS on smartphone to obtain vehicle speed. The limitation of technique is that it suffers from urban canyon environment and the performance of the sampling-based estimation may also suffer in environment with a small number of samples only.

B. Road Condition Surveillance Using Magnetometers

Recently, a number of researchers considered vehicle detection and speed estimation methods using magnetic sensors [10], [16]–[21]. Balid [22] deployed multiple on-road sensors for traffic surveillance. Their work can successfully detect vehicles and estimate varying speeds of vehicles through a set of magnetic sensors deployed along the road.

Reference [23] reported 90% of the average speed estimation precision through measuring magnetic length using a roadside node with an accelerometer and magnetic sensor. Taghvaeeyan in [10] proposed applying four magnetic sensors for vehicle counting and vehicle speed measurement, respectively, which resulted in 95% classification accuracy and the maximum error of the speed estimates is less than 2.5% over the entire range of 5–27 m/s. The technique in [11] adopted two magnetic sensors for vehicle speed estimation and a third magnetic sensor for data fusion, which resulted in a speed estimation accuracy of 80%. Studies in [24] and [25] developed algorithms for speed estimation using two magnetometers. It is worth noting that these methods needed to first estimate the average speed based on the number of passing vehicles over time, which could be difficult to acquire. Vehicle detection and classification through an improved support vector machine classifier was proposed in [26] using magnetic sensors. They used magnetic signatures to distinguish different types of vehicles, such as heavy trucks and light-wheeled vehicles. However, the algorithm is time-consuming, which required high processing capability to get 80% to 90% accuracy. The work in [21] first analyzed the magnetic effect of vehicle's metal body and simulated a scenario to detect a vehicle using magnetic sensors. Cheung, Ergen and Varaiya in [27] developed a feature selection model for vehicle classification by a line of wireless sensors. There are also works on using combination of magnetic sensors for vehicle information acquisition. Studies in [19], [24], [28]–[30] proposed vehicle classification based on machine learning of the signal waveforms.

Obtaining the vehicle speed is becoming increasingly important in supporting real-time traffic management. In the aforementioned studies, speed was estimated using two or more magnetic sensors. References [22] and [31] focused on vehicle classification by multiple magnetic sensors or with the combination of accelerometers.

Our work is distinct from the previous studies in that we investigate using a single magnetic sensor approach for vehicle classification and speed estimation in a non-intrusive way.

III. Methodology

In this section, we present the design of the proposed system, MagMonitor, which detects vehicles and estimates vehicle speeds through measuring and modelling local magnetic field perturbation caused by moving vehicles. The deployment of MagMonitor only requires a small magnetic sensor to be placed on the roadside. We first explain the working mechanism of a metal object's magnetic characteristics in *Section A*, then describe the motion process of moving vehicles in *Section B* and present the models for vehicle speed estimation. Signal processing to remove background noise and provide vehicle moving time is illustrated in *Section C*. We analyze the lateral effects in *Section D* and the impact of vehicle moving directions in *Section E*, and apply them to gain accurate estimates with real field experimental data. After we gain the traffic volumns from the magnetic perturbation, *Section F* explains the classification of vehicle types from the magnetic perturbation dataset using image-based processing methods. In summary, we start from the methodology and experimental observation characteristics, and include consideration of the issues to separate vehicle perturbation, finally vehicle types and vehicle speed estimation will be achieved.

A. Multiple Magnetic Dipole Models

For a moving vehicle with a constant velocity, it comprises a huge amount of ferromagnetic materials and will induce a magnetic field. With the development of modern sensor techniques, the electromagnetic field $\boldsymbol{B}$ can be measured through a geomagnetic sensor.

Based on the electromagnetic theory, if the distance to the metallic object is large enough in comparison to its characteristic length, the moving metallic object can be modeled as a magnetic dipole.

For a magnetic dipole located at a distance r from the origin, its magnetic field at the origin can be expressed as [32], [33]:

$$\boldsymbol{B} = \begin{pmatrix} 3x^2 - r^2 & 3xy & 3xz \\ 3xy & 3y^2 - r^2 & 3yz \\ 3xz & 3yz & 3z^2 - r^2 \end{pmatrix} \bullet \frac{u_0 \boldsymbol{m}}{4\pi r^5}. \quad (1)$$

where $\boldsymbol{m}$ is the magnetic moment of a dipole, u_0 is magnetic permeability with a value of $4\pi \times 10^{-7} H/m$, r is the distance between the measurement position at the origin and the magnetic dipole at coordinate (x, y, z), with $r^2 = x^2+y^2+z^2$. The tensor notation of the equation in the orthogonal coordinate system will take the following form with the expansion of magnetic vector being $\boldsymbol{m} = \begin{pmatrix} \boldsymbol{m_x} & \boldsymbol{m_y} & \boldsymbol{m_z} \end{pmatrix}^{\boldsymbol{T}}$, where m_x, m_y, m_z are the component of the magnetic moment on the $x-axis$, $y-axis$, $z-axis$, respectively, and $\bullet$ means dot product. It follows from (1) that the three magnetic component along the $x-axis$, $y-axis$, and $z-axis$ can be written as:

$$\begin{aligned} B_x &= \left(\left(3x^2 - r^2\right) \cdot m_x + 3xy \cdot m_y + 3xz \cdot m_z\right) \cdot \frac{u_0}{4\pi r^5}, \\ B_y &= \left(3xy \cdot m_x + \left(3y^2 - r^2\right) \cdot m_y + 3yz \cdot m_z\right) \cdot \frac{u_0}{4\pi r^5}, \\ B_z &= \left(3xz \cdot m_x + 3yz \cdot m_y + \left(3z^2 - r^2\right) \cdot m_z\right) \cdot \frac{u_0}{4\pi r^5}. \end{aligned} \quad (2)$$

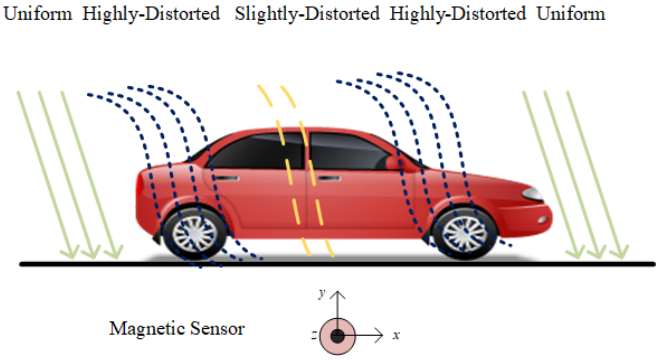

Fig. 1. Magnetic perturbation caused by a vehicle [22].

For the magnetic field value of $x-axis$, $y-axis$ and $z-axis$, respectively, we expand the value of r and simplify the expression of B_x, B_y, B_z as follows:

$$\begin{aligned} B_x &= \left(\left(2x^2 - y^2 - z^2\right) \cdot m_x + 3xy \cdot m_y + 3xz \cdot m_z\right) \\ &\quad \cdot \frac{u_0}{4\pi \left(x^2 + y^2 + z^2\right)^{\frac{5}{2}}}, \\ B_y &= \left(3xy \cdot m_x + \left(2y^2 - x^2 - z^2\right) \cdot m_y + 3yz \cdot m_z\right) \\ &\quad \cdot \frac{u_0}{4\pi \left(x^2 + y^2 + z^2\right)^{\frac{5}{2}}}, \\ B_z &= \left(3xz \cdot m_x + 3yz \cdot m_y + \left(2z^2 - x^2 - y^2\right) \cdot m_z\right) \\ &\quad \cdot \frac{u_0}{4\pi \left(x^2 + y^2 + z^2\right)^{\frac{5}{2}}}. \end{aligned} \quad (3)$$

Considering a small vehicle with a certain speed driving on the road along the $+x-axis$, it leads to perturbations of the local magnetic fields and the small vehicle can be modelled as a magnetic dipole [34]. Fig. 1 (in Section II) [22] illustrates the magnetic distribution of the magnetic flux lines when the earth's magnetic field is temporarily changed by a car. It shows that the magnetic fields are highly distorted at the wheels and slightly distorted at other parts. The unit for time measurement in this paper is second.

Furthermore, for multiple magnetic dipole case, the equation becomes :

$$\boldsymbol{B}(L) = \textstyle\sum_i \boldsymbol{B}_i(L) \quad (4)$$

where i is the magnetic dipole index of the $i-th$ dipole. Because the magnetic moment has a direction and it has values along $x-axis$, $y-axis$, and $z-axis$, we can set a default $m = (1, 1, 1)$ for initial simulation [32], [35]–[37] to focus on studying the magnetic field variation.

Intuitively, the longer the vehicle is, the more number of magnetic dipoles should be used. For heavy and long vehicles with a certain speed, each vehicle can be modelled by two or more magnetic dipoles in order to represent its magnetic field perturbation accurately. The simulations of each axis are displayed as in Figs. 2 (a) - (d) to present the effect of the varying numbers of magnetic dipoles. The total magnetic moment for vehicles can't be measured directly. According

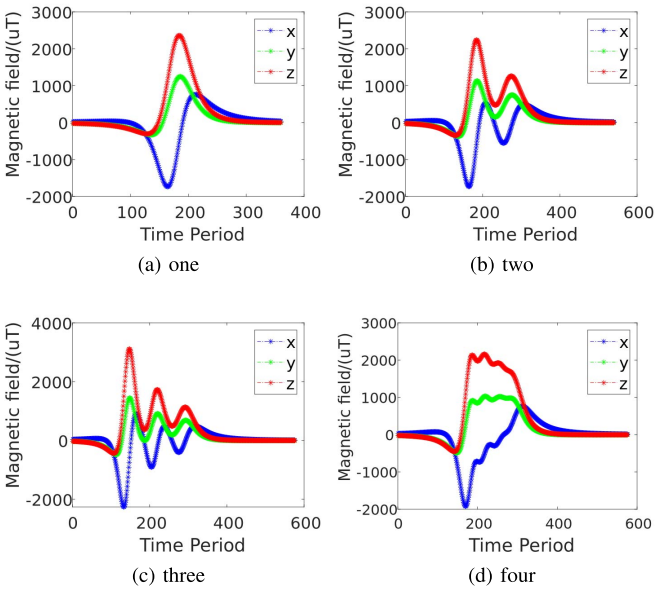

(a) one (b) two (c) three (d) four

Fig. 2. Using one, two, three and four magnetic dipoles for vehicle simulation.

to [21], a typical U.S. automobile has a magnetic moment in the range 100-300 A/m^2(Ampere-meter^2), while for a school bus it is about 2000 A/m^2. So we consider an average value 200 A/m^2 in the range 100-300 A /m^2 [16] for simulation of a small car. Through the modelling from (4), we demonstrated that the variations of magnetic waveforms provide evidence for the length of vehicles. For SUVs and van, two magnetic dipoles should be enough. For a small bus, three magnetic dipoles are more appropriate. For a long bus and truck, they should be represented by four magnetic dipoles. The intuition are verified by the results of real experiment magnetic data. Please see the example in Fig. 20 from Appendix.

B. Moving Vehicle Motion Models

In this part, we establish and analyze the motion model for a driving vehicle. The discrete state space model of a moving vehicle is illustrated as follows:

$$\begin{aligned} \boldsymbol{r}_{k+1} &= \boldsymbol{r}_k + t \cdot \boldsymbol{v}_k + \frac{t^2}{2} \cdot \boldsymbol{w}_k, \\ \boldsymbol{v}_{k+1} &= \boldsymbol{v}_k + t \cdot \boldsymbol{w}_k, \\ \boldsymbol{m}_{k+1} &= \boldsymbol{m}_k. \end{aligned} \tag{5}$$

where $\boldsymbol{r}_k$ means the position vector for a target vehicle, with speed $\boldsymbol{v}_k$ and acceleration $\boldsymbol{w}_k$ for the $k-th$ state, t is the time interval between the $k-th$ state and the $k+1-th$ state, $\boldsymbol{m}_k$ is the magnetic moment. A three-dimensional Cartesian coordinate system is set up from the view of the magnetic sensor, which is at the origin $(0, 0, 0)$. Consider a vehicle driving on a straight road with a speed of $\boldsymbol{v}_k$ ($\boldsymbol{v}_k > 0$) along the $x-axis$, and an initial position (x_0, y_0, z_0). Only the $x-axis$ has speed, so $\boldsymbol{v}_k = \boldsymbol{v}_x$. The initial value of x_0 is negative and it is the first position that causes the local magnetic perturbation, the initial value of y_0 is zero and the initial value of z_0 is a small and non-negative value, representing that the sensor is placed on the roadside and hence has some distances from the vehicle. After a period of time t ($t > 0$), the vehicle's location becomes $(x_0 + \boldsymbol{v}_x \cdot t, y_0, z_0)$. The magnetic moments of the vehicle, denoted by $\boldsymbol{m}_k = \begin{pmatrix} \boldsymbol{m}_x & \boldsymbol{m}_y & \boldsymbol{m}_z \end{pmatrix}$, observed at the sensor position become:

$$\begin{aligned} y = \frac{u_0}{4\pi r^5} \cdot \begin{pmatrix} \boldsymbol{m}_x \\ \boldsymbol{m}_y \\ \boldsymbol{m}_z \end{pmatrix} \bullet \\ \begin{pmatrix} 3(x_0 + \boldsymbol{v}_x \cdot t)^2 - r^2 & 3(x_0 + \boldsymbol{v}_x \cdot t)y_0 & 3(x_0 + \boldsymbol{v}_x \cdot t)z_0 \\ 3(x_0 + \boldsymbol{v}_x \cdot t)y_0 & 3y_0^2 - r^2 & 3y_0 z_0 \\ 3(x_0 + \boldsymbol{v}_x \cdot t)z_0 & 3y_0 z_0 & 3z_0^2 - r^2 \end{pmatrix} \end{aligned} \tag{6}$$

Then, the expansion for y_x is given by:

$$\begin{aligned} y_x &= 2\left(x_0 + \boldsymbol{v}_x \cdot t\right)^2 \cdot m_x \cdot \frac{u_0}{4\pi\left(\left(x_0 + \boldsymbol{v}_x \cdot t\right)^2 + D\right)^{\frac{5}{2}}} \\ &\quad + 3\boldsymbol{v}_x \cdot t \cdot y_0 \cdot m_y \cdot \frac{u_0}{4\pi\left(\left(x_0 + \boldsymbol{v}_x \cdot t\right)^2 + D\right)^{\frac{5}{2}}} \\ &\quad + 3\boldsymbol{v}_x \cdot t \cdot z_0 \cdot m_z \cdot \frac{u_0}{4\pi\left(\left(x_0 + \boldsymbol{v}_x \cdot t\right)^2 + D\right)^{\frac{5}{2}}} \\ &\quad + C \cdot \frac{u_0}{4\pi\left(\left(x_0 + \boldsymbol{v}_x \cdot t\right)^2 + D\right)^{\frac{5}{2}}} \\ &= \frac{\mathrm{A} \cdot \left(x_0 + \boldsymbol{v}_x \cdot t\right)^2 + B \cdot \boldsymbol{v}_x \cdot t + C}{\left(x_0 + \boldsymbol{v}_x \cdot t\right)^5 + D} \end{aligned} \tag{7}$$

where $A = 2\frac{m_x \cdot u_0}{4\pi}$,

$$\begin{aligned} B &= 3\frac{z_0 \cdot m_z \cdot u_0}{4\pi}, \\ C &= \frac{3x_0 \cdot z_0 \cdot m_z \cdot u_0 - z_0^2 \cdot m_x \cdot u_0}{4\pi}, \\ D &= \left(\left(x_0 + \boldsymbol{v}_x \cdot t\right)^2 + z_0^2\right)^{\frac{5}{2}} \\ &\quad - \left(x_0 + \boldsymbol{v}_x \cdot t\right)^5 \end{aligned}$$

Since z_0 can be assumed to be small, the values of B and C are also small and can be neglected. Thus, an approximation can be applied and y_x can be rewritten as:

$$y_x = \frac{A \cdot \left(x_0 + \boldsymbol{v}_x \cdot t\right)^2}{\left(x_0 + \boldsymbol{v}_x \cdot t\right)^5 + D} \tag{8}$$

Let $h(t) = y_x$, and let the reciprocal of $h(t)$ be $g(t) = \frac{1}{h(t)}$, then

$$g(t) = \frac{\left(x_0 + \boldsymbol{v}_x \cdot t\right)^5 + D}{A \cdot \left(x_0 + \boldsymbol{v}_x \cdot t\right)^2} \tag{9}$$

Meanwhile, letting $\boldsymbol{v}_x \cdot t = x$, x reflects the change of positions with a speed v_x during the time period. Because $\boldsymbol{v}_x > 0$ and $t > 0$, so $x > 0$, so we have

$$\begin{aligned} g(x) &= \frac{1}{A}(x_0 + x)^3 + \frac{D}{A(x_0 + x)^2} \\ &= \frac{1}{A}x^3 + \frac{3x_0}{A}x^2 + \frac{3x_0}{A}x + \frac{{x_0}^3}{A} + \frac{D}{A(x_0 + x)^2} \end{aligned} \tag{10}$$

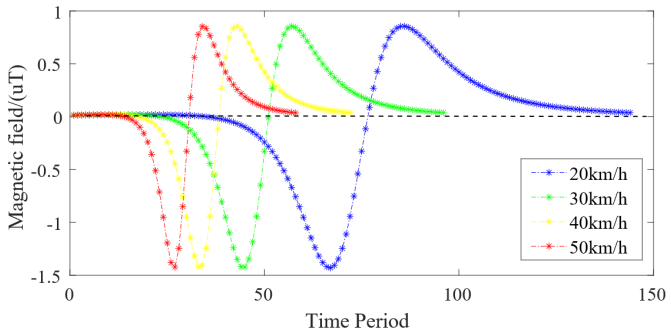

Fig. 3. Simulation of x axis from 20 km/h to 50 km/h.

As the value of x $(x > 0)$ increases, $\frac{1}{A}x^3 + \frac{3x_0}{A}x^2 + \frac{3x_0}{A}x + \frac{{x_0}^3}{A}$ increases, and $\frac{D}{A(x_0+x)^2}$ decreases. There is a turning point that $g(x)$ reaches its minimum value at $x = \sqrt[5]{-D} - x_0$.

If $x < \sqrt[5]{-D} - x_0$, the dominating term for $g(x)$ is $\frac{D}{A(x_0+x)^2}$, thus $g(x) = \frac{D}{A(x_0+x)^2} + \varepsilon_1$, where ε_1 is the residual error.

If $x = \sqrt[5]{-D} - x_0$, $g(x) = 0$.

If $x > \sqrt[5]{-D} - x_0$, the dominating term for $g(x)$ is $\frac{1}{A}(x_0 + x)^3$, thus $g(x) = \frac{1}{A}(x_0 + x)^3 + \varepsilon_2$, where ε_2 is the residual error. Based on the above analysis, (12) can be rewritten as:

$$g(x) = \begin{cases} \dfrac{D}{A(x_0+x)^2} + \varepsilon_1 & x < \sqrt[5]{-D} - x_0 \\ 0 & x = \sqrt[5]{-D} - x_0 \\ \dfrac{1}{A}(x_0 + x)^3 + \varepsilon_2 & x > \sqrt[5]{-D} - x_0 \end{cases} \tag{11}$$

Through the analysis of $g(x)$, there are four approximations models of $f(t)$ given as follows:

Model 1: power form

$$f_1(t) = at^b + c + \varepsilon_1 \tag{12}$$

Model 2: polynomial form

$$f_2(t) = a_0 + a_1 t + a_2 t^2 + a_3 t^3 + \ldots + a_n t^n + \varepsilon_2 \tag{13}$$

Model 3: rational form

$$f_3(t) = \frac{p_1}{t^3 + q_1 t^2 + q_2 t + q_3} + \varepsilon_3 \tag{14}$$

Model 4: combination of polynomial form and rational form

$$f_4(t) = \lambda_1 t^3 + \lambda_2 t^2 + \lambda_3 t + \lambda_4 + \lambda_5 (t^{(-3)}) + \varepsilon_4 \tag{15}$$

Fig. 3 gives the magnetic waveform corresponding to different speed of a magnetic dipole moving along the $x-axis$, which varies between 20 km/h to 50 km/h. As can be seen from the figure, with different vehicle speeds, the time window for the detected magnetic distortion is changing.

Here we analyze whether there is a turning point to ensure B_x induced by a vehicle reaches its minimum. Defining $B_x = \frac{n_1(t)}{n_{2(t)}} = \frac{A\cdot(x_0+\boldsymbol{v}_x\cdot t)^2}{(x_0+\boldsymbol{v}_x\cdot t)^5+D}$, the derivative of B_x then can be given by:

$$\frac{\partial B}{\partial t} = \left(\frac{n_1'(t)n_2(t) - n_1(t)n_2'(t)}{[n_2(t)]^2} \right) \tag{16}$$

For x, we have

$$\begin{aligned} & n_1'(t)n_2(t) - n_1(t)n_2'(t) \\ &= [2A\,(x_0 + \boldsymbol{v}_x t)\cdot \boldsymbol{v}_x][(x_0 + \boldsymbol{v}_x t)^5 + D] \\ &\quad - [A\cdot(x_0 + \boldsymbol{v}_x t)^2][5\boldsymbol{v}_x\,(x_0 + \boldsymbol{v}_x t)^4] \\ &= [2A\boldsymbol{v}_x\,(x_0 + \boldsymbol{v}_x t)^6 + D] - 5A\boldsymbol{v}_x\,(x_0 + \boldsymbol{v}_x t)^6 \\ &= -3A\boldsymbol{v}_x\,(x_0 + \boldsymbol{v}_x t)^6 + 2AD\boldsymbol{v}_x\,(x_0 + \boldsymbol{v}_x t) \end{aligned} \tag{17}$$

Because

$$\frac{\partial B}{\partial t} = 0 \Rightarrow n_1'(t)n_2(t) - n_1(t)n_2'(t) = 0$$

it follows that

$$\begin{aligned} 3\,(x_0 + \boldsymbol{v}_x t)^5 &= 2D \\ x_0 + \boldsymbol{v}_x t &= \sqrt{\frac{2D}{3}} \\ t &= \frac{\sqrt[5]{\frac{2D}{3}} - x_0}{\boldsymbol{v}_x} \end{aligned} \tag{18}$$

Since it is the fifth-order polynomial, there is at least one solution of t to make $\frac{\partial B}{\partial t} = 0$. Consequently, there is a t resulting in B_x reaching its minimum/maximum, and in Fig. 3, it is verified as a minima/maxima. For the derivatives of B_y and B_z, they are similar to B_x.

Now the relationships between time and the magnetic field perturbation caused by a moving vehicle are given in equations (16) - (18). If we combine the models with time t, the parameters above can be calculated accordingly. There is a value t_0 resulting in $B_x = 0$, which is the point that allows $f(t) = 0$. For different speeds, t_0s are different, which reflects the intervals between the beginning of x-axis and the time at $B_x = 0$. Given different t_0s, it then relates to the driving speed of the vehicles respectively, which leads to the estimation of vehicle speed. Note that the t_0s are obtained from real-time traffic data after filtering of environmental noise. The signal processing technique and filter techniques are introduced in the next section. Experimental results for the models are given in Section IV. From the above analysis, $-\frac{x_0}{v_x}$ can reflect the magnetic vibration response time for vehicles, while different x_0s depends on different types of vehicles. So for different vehicle types, speed estimation can be achieved given the time-varying magnetic perturbation vectors.

C. Signal Processing Model

Measurements in real road condition are full of background noises and are affected by earth's magnetic field [34]. It makes the signals hard to distinguish for the passing vehicles. So a low-pass filter is first applied [26].

The local earth's magnetic value are B_{x0}, B_{y0}, B_{z0}, which are relatively stable values in this paper. Moreover, the values can be obtained from the roadside magnetic sensor when there is no vehicle passing by. $\left(B_{xk}, B_{yk}, B_{zk}\right)$ are the values recorded by the magnetic sensor when a vehicle is passing. $\left(B_{vx}, B_{vy}, B_{vz}\right)$ is the perturbation caused by a passing vehicle, then:

$$\left(B_{vx}, B_{vy}, B_{vz}\right) = \left(B_{xk} - B_{x0}, B_{yk} - B_{y0}, B_{zk} - B_{z0}\right) \tag{19}$$

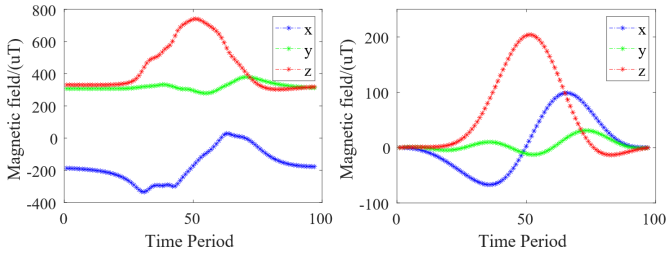

(a) Before the processing (b) After the processing

Fig. 4. An example of the signal processing with real magnetic data of a 30 km/h vehicle. We first apply equation (20) and remove the local earth's magnetic value, here $B_{x0}, B_{y0}, B_{z0} = (-185, 310, 347)$ from (a). Then, we apply low-pass filter to gain a pure vehicle magnetic vibration waveforms as shown in (b).

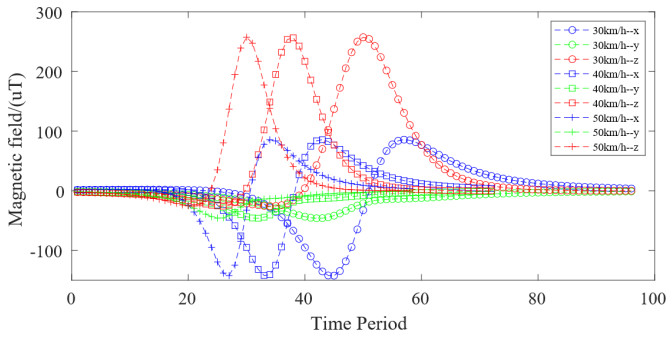

Fig. 5. Simulation on a magnetic dipole moving from 30 km/h to 50 km/h.

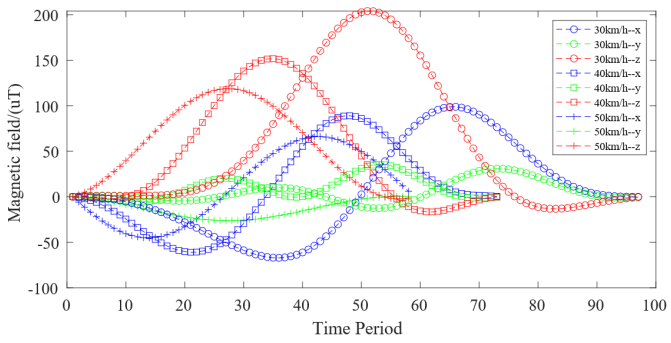

Fig. 6. Filtered and normalized real-time data from 30 km/h to 50 km/h.

Fig. 4 (a) shows the waveform of (B_{xk}, B_{yk}, B_{zk}) for a vehicle travelling at 30 km/h speed. There are lots of noises in real environment. Besides reducing the (B_{x0}, B_{y0}, B_{z0}), we apply Fast Fourier Transform (FFT) and on that basis develop a first-order low pass filter with a cut off frequency at 5 Hz for (B_{vx}, B_{vy}, B_{vz}) to remove noise effect, which allows low frequency signals in frequency domain to pass. So after the FFT signal processing, Fig. 4 (b) shows the filtered and normalized waveforms by FFT for a vehicle at a speed of 30 km/h. Fig. 5 and Fig. 6 are the simulations of a vehicle with speed varying from 30 km/h to 50 km/h and the corresponding filtered normalized real data of respectively. Through signal processing, it aims to easier extraction of $\boldsymbol{t_0}$.

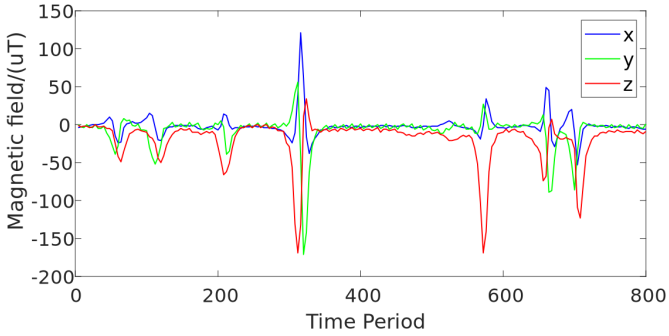

(a) Real-time data of normalized vehicle's magnetic perturbation.

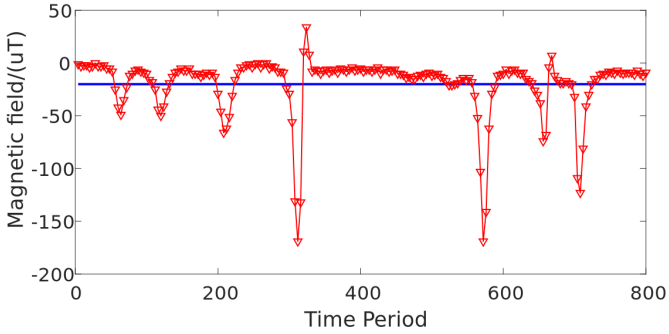

(b) Combined real-time data of normalized vehicle's magnetic perturbation.

Fig. 7. Magnetic data combination.

D. Lateral Effect Influences on Magnetic Perturbation

What needs to be considered to count vehicles in the real world field test is, the vehicles driving in the adjacent road can always be calculated as wrong detection. So the combination of three axis signals would be employed to reduce the false vehicle detection.

$$B_{combination} = \sqrt{(B_x)^2 + (B_y)^2 + (B_z)^2} \tag{20}$$

Here, we process experimental data applying the proposed method in Figs. 7 (a) and (b) for easy understanding. There are multiple vehicles driving on the experimental road, as seen after the combination processing, the vehicle magnetic signature above the threshold will be counted.

For a driving vehicle, the distance between the sensor and the vehicle is a crucial issue affecting the vibration of the vehicle. We consider a vehicle driving along a line parallel to the roadside. For vehicles in different lanes, the lateral distances are changed. So we add lateral influences into consideration, and Figs. 8 reflects how the factor has an influence on the signal changes.

Here we want to know the effects of lateral distances changing from a small value to a relative big value. $d = 0.2$ m is chosen to represent the sensor mounted on the lane in which a vehicle is moving, and $d = 2$ m is chosen to approximately represent the vertical distance between the roadside sensor and the center of the closest lane to the sensor. $d = 4$ m is approximate the distance between the side of the adjacent lane and the sensor, and $d = 6$ m is the approximate distance between the side line of the adjacent lane to the sensor.

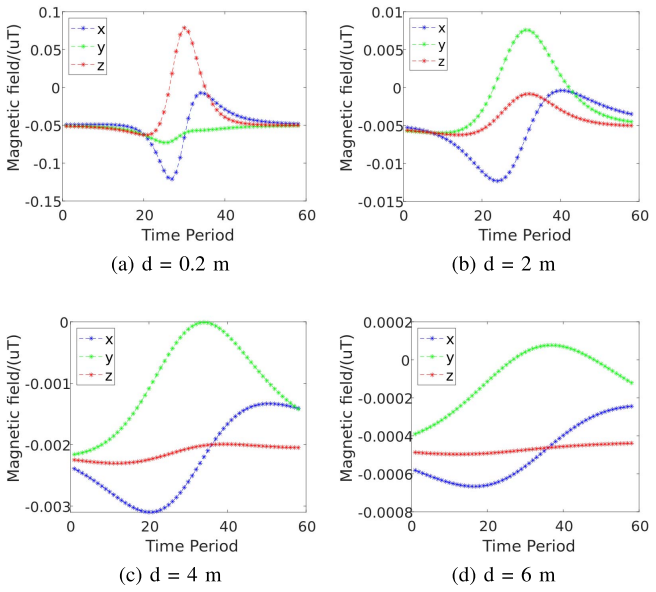

(a) d = 0.2 m (b) d = 2 m

(c) d = 4 m (d) d = 6 m

Fig. 8. Lateral effects between the sensor and the vehicle.

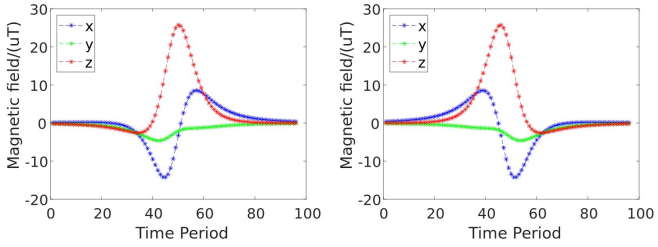

(a) Moving towards the sensor (b) Moving away from the sensor

Fig. 9. Vehicle driving in different directions.

Note that as the value of d increases, the order of magnetic perturbation decreases, which makes it easy to separate the perturbations. In other words, if a vehicle drives on the adjacent lane, then its magnetic perturbation waveforms will be flat as shown in Figs. 8 (c) - (d).

E. Vehicle Moving Direction Analysis

There is a practical interference needing to be considered: the relative position of the magnetic sensor and the passing vehicles. If the vehicle moving direction is not aligned with the coordinate system, corresponding magnetic perturbation is changed. Figs. 9 is a visual reflection for the aforementioned problem. It shows that for a vehicle driving at a constant speed, the direction of perturbation changes with the driving directions.

F. Vehicle Type Classification Method

The principle of vehicle type classification is based on image processing. After we obtain vehicle volume from the previous section, we put the magnetic perturbation images into the vehicle perturbation dataset. As mentioned in the magnetic dipole models part, magnetic perturbations differ from the various number of the magnetic dipoles and response time of driving vehicles, which results in different signal shapes such as the number of maxima and length of vibration. These features can be used for vehicle type classification. For example, when using the vehicle magnetic perturbation images to train, the image-based classification can directly extract the features in each types. Then, we put the test images to test the classification rate, we can get the score of its likelihood in each type directly, which is convenient.

Algorithm 1 is the algorithm for vehicle type classification. The training dataset consists of magnetic signal images caused by driving vehicles, and the testing dataset is separate from the training dataset for vehicle information. It can output the labels of predicted types of vehicles. Through loading training dataset, resizing the images and extracting histogram of oriented gradients (HOG) features, the classifier is established for feature testing. Then loading the testing dataset, do the same resizing and extracting features as the training dataset. We apply the fitcecoc in Matlab to construct the classifier, which is a function that suits multi-class models for classifiers like support vector machines (SVM). Then we use the classifier trained by the training dataset, and compare the features with each label. Therefore the magnetic perturbations caused by different categories of vehicles are classified.

Algorithm 1 The Algorithm for Vehicle Type Classification

Input : The training dataset $imdsTrain$;
The testing dataset $imdsTest$
Output : Vehicle type prediction index n

```
Load imdsTrain and imdsTest into imageDataStore
for images in imdsTrain
    Image resize imresize in each label
    through feature extraction extractHOGFeature
    Feature train featuresTrain
end for
Use fitcecoc to build classifier
for images in imdsTest
    Image resize imresize
    through feature test extractHOGFeature
    Test with classifier
end for
```

IV. Evaluation

In this section, we present the evaluation of our vehicle classification and vehicle speed estimation technique, MagMonitor, with real driving environments. Here we describe the experiment setup, the results of assumption models and evaluate vehicle speed estimation errors. Contrast experiments for the speed estimation error with techniques in the literature.

A. Experiment Setup

We evaluate MagMonitor, in real driving environments in a road in Xi'an, China. Fig. 10 (a) is a RM3100 magnetic sensor, which outputs magnetic vibration along three axes. The size of the chip is only as large as a coin and the overall size of the sensor is tiny, which is portable for traffic surveillance. In addition, a magnetic sensor costs as cheap as 30 dollars.

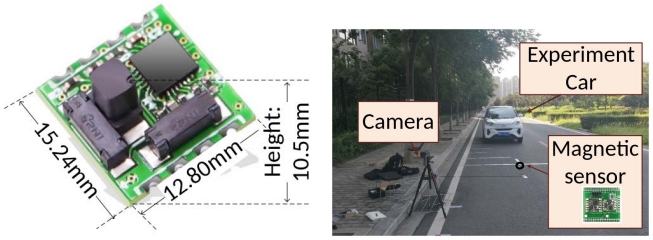

(a) Sensor (b) A sedan test

Fig. 10. Sensor design and a sedan test.

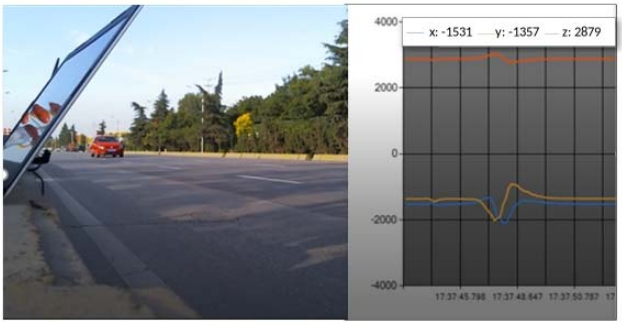

Fig. 11. Experiment setup on the left and the display board on the right.

Also, a camera is put on roadside to record the overall driving period. Fig.10 (b) shows an experiment setup on the road, which is an example for the test of a sedan type vehicle from our previous work in [38].

After the initial experiment for the sedan type vehicle, multiple experiments are conducted. In Fig. 11, the left records the road for vehicle magnetic signatures, and the right is the real-time sensor's display board recording magnetic values for driving vehicles. The right side of Fig.11, magnetic perturbation matches the theoretical analysis in Sec. III well. The real vehicle speeds are measured by a speedometer.

Our previous work in [39] introduced the detection methods and the experiment of the vehicle numbers. According to the standard of [7], we classify the recorded vehicles into four types: sedan, SUV and van, bus and truck. After the magnetic data is preprocessed, the measured vehicles' magnetic signals are extracted into separate images for classification. Overall, 115 vehicle profile is randomly selected into a training dataset of 58 vehicles and a testing dataset of 57 vehicles.

Furthermore, we have also conducted the experiments at different locations, in different seasons and weathers. There is no evidence that the season and weather affects much during our experiments.

B. Experimental Results

Here we classify our experiment results into two parts: vehicle classification and vehicle speed estimation.

For vehicle classification, as shown in Table I, the diagonal values are the classification rates for testing dataset. Through applying the vehicle type classification technique mentioned in III. F, we then get the correct classification rate of 87%,

TABLE I
VEHICLE CLASSIFICATION RESULT IN FOUR TYPES

CR	sedan	SUV and van	bus	truck
sedan	95	5	0	0
SUV and van	7	79	7	7
bus	0	0	96	4
truck	0	9	0	91

TABLE II
VEHICLE CLASSIFICATION RESULT IN THREE TYPES

CR	sedan	SUV	bus
sedan	93	3.5	3.5
SUV	0	96	4
bus	9	0	91

initially. As shown in the table, the classification rate for sedan, bus and truck are all more than 90%, but the classification rate for SUV and van is much lower compared to other vehicle types. The reason for the low classification results is that these two types of vehicles are similar. So here we combine the middle two types into one type. After applying that strategy, the classification performance is shown in Table II. For comparison, the work in [26] evaluates BPNN and KNN classifiers for heavy tracked vehicle, light tracked vehicle, light wheeled vehicle. For BPNN classifier, three types' recognition rates are 81.5%, 78.6%, 76.3% and KNN classifier 77.8%, 71.4%, 71.1% respectively. In comparison, our image-based classification rates are 91%, 96%, 93%, which significantly outperforms the BPNN and KNN classifiers.

To gain the estimated vehicle speeds, we separate the speed estimation models in section III and contrast them with real speeds. In three vehicle types, we estimate values of each fitting models through separating the times of driving vehicles. The parameters are calculated by Matlab R2019 on windows 10 as follows.

(1) The vehicle speed estimation models for sedan:

For power form, $f_1(t) = at^b + \varepsilon_1$. Coefficients (with 95% confidence bounds): $a = 29.54, b = -0.8788$.

For polynomial form, $f_2(t) = a_0 + a_1 t + a_2 t^2 + a_3 t^3 + \varepsilon_2$. Coefficients (with 95% confidence bounds): $a_0 = 93.09$, $a_1 = -112.8, a_2 = 59.26, a_3 = -12.19$.

For rational form, $f_3(t) = \frac{p_1}{t^3 + q_1 t^2 + q_2 t + q_3} + \varepsilon_3$. Coefficients (with 95% confidence bounds): $p1 = 16.61$, $q1 = -2.415, q2 = 2.365, q3 = -0.4033$.

For combination form, $f(t) = \lambda_1 t^3 + \lambda_2 t^2 + \lambda_3 t + \lambda_4 + \lambda_5 (t^{(-3)}) + \varepsilon_4$. Coefficients (with 95% confidence bounds): $\lambda_1 = 293.3, \lambda_2 = -962.8, \lambda_3 = 1032, \lambda_4 = -345$, $\lambda_5 = 11.58$.

(2) The vehicle speed estimation models for SUVs and vans:

For power form, $f_1(t) = at^b + c + \varepsilon_1$. Coefficients (with 95% confidence bounds): $a = 203.3, b = -0.14, c = -165.5$.

For polynomial form, $f_2(t) = a_0 + a_1 t + a_2 t^2 + a_3 t^3 + \varepsilon_2$. Coefficients (with 95% confidence bounds): $a_0 = 78.25$, $a_1 = -47.13, a_2 = 4.742, a_3 = 2.2181$.

For rational form, $f_3(t) = \frac{p_1}{t^3 + q_1 t^2 + q_2 t + q_3} + \varepsilon_3$. Coefficients (with 95% confidence bounds): $p1 = 709.3$, $q1 = 0.1174, q2 = 11.06, q3 = 6.543$.

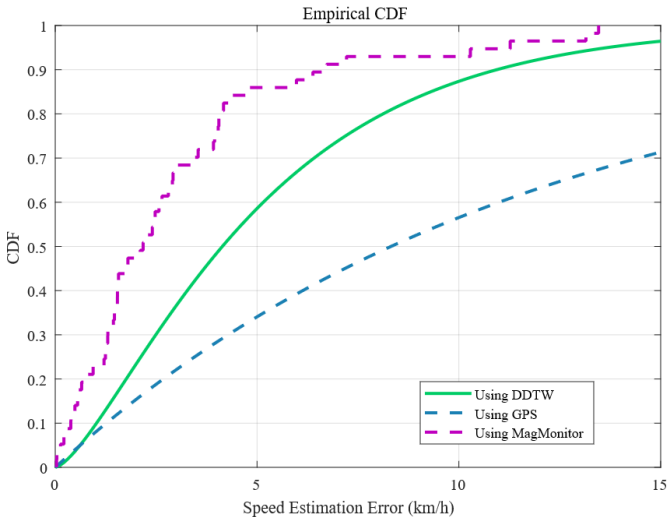

Fig. 12. CDF of the speed estimation errors for sedans.

For combination form, $f(t) = \lambda_1 t^3 + \lambda_2 t^2 + \lambda_3 t + \lambda_4 + \lambda_5(t^{(-3)}) + \varepsilon_4$. Coefficients (with 95% confidence bounds): $\lambda_1 = 53.81, \lambda_2 = -225.1, \lambda_3 = 287.9, \lambda_4 = -85.27, \lambda_5 = 7.508$.

(3) The vehicle speed estimation models for buses and trucks:

For power form, $f_1(t) = at^b + \varepsilon_1$. Coefficients (with 95% confidence bounds): $a = 58.04, b = -0.8677$.

For polynomial form, $f_2(t) = a_0 + a_1 t + a_2 t^2 + a_3 t^3 + \varepsilon_2$. Coefficients (with 95% confidence bounds): $a_0 = 92.92, a_1 = -46.63, a_2 = 9.722, a_3 = -0.8219$.

For rational form, $f_3(t) = \frac{p_1}{t^3+q_1 t^2+q_2 t+q_3} + \varepsilon_3$. Coefficients (with 95% confidence bounds): $p1 = 391200, q1 = 1746, q2 = -92.31, q3 = 5483$.

For combination form, $f(t) = \lambda_1 t^3 + \lambda_2 t^2 + \lambda_3 t + \lambda_4 + \lambda_5(t^{(-3)}) + \varepsilon_4$. Coefficients (with 95% confidence bounds): $\lambda_1 = -11.79, \lambda_2 = 83.32, \lambda_3 = -210.8, \lambda_4 = 217.6, \lambda_5 = -24.64$.

In addition, the vehicle estimation model is based on the training dataset and test on the testing dataset. The mis-classified vehicles have an impact on the speed estimation accuracy. In other words, the mis-classified vehicles are calculated using the types that they are considered as.

C. Discussion

Here we first discuss the proposed models for speed estimation in sedan, because the number of sedans is larger than other vehicle types. Fig. 12 plots the cumulative distribution function (CDF) of the speed estimation errors (km/h) for the proposed technique, Derivative Dynamic Time Warping (DDTW) [40] and GPS. The results explain that we achieve high speed estimation performance in the proposed models. For example, 80% of estimation errors are lower than 4 km/h if using the four proposed models, and 50% of estimation errors are less than 2.5 km/h. In addition, only 8% of the estimated speed errors exceeds 10 km/h. The average estimation errors include all the vehicle types mentioned in this paper. Thus,

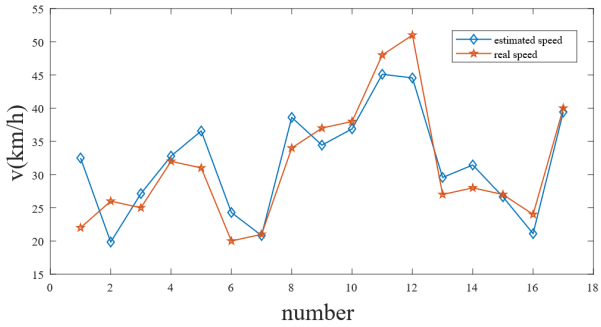

Fig. 13. Sedan speed experiments comparison.

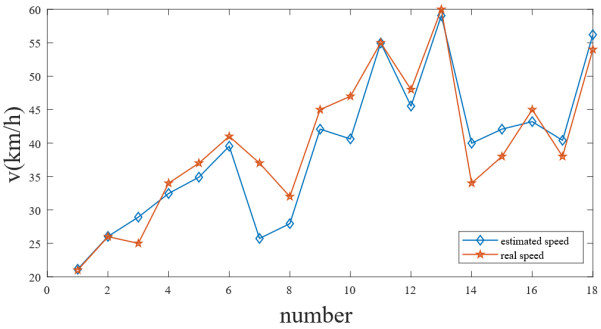

Fig. 14. SUVs and vans speed experiments comparison.

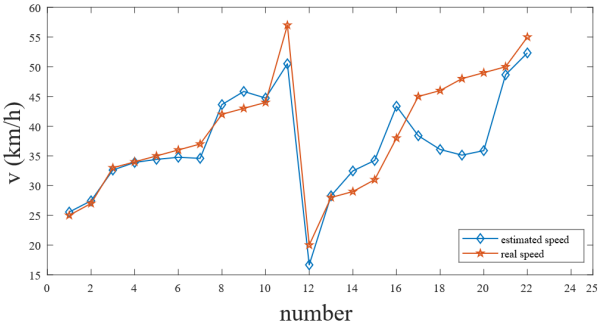

Fig. 15. Buses and trucks speed experiments comparison.

the proposed fitting models are robust for vehicle speed estimation. In the meantime, we compare the four proposed models with DDTW and GPS. From Fig. 12, it can be seen that the fitting models outperforms GPS in speed estimation. Compared with DDTW, the fitting models still outperforms. For example, 90% of DDTW's estimation errors are less than 11 km/h. By contrast, 90% of the estimation errors for the proposed models are lower than 7.5 km/h.

D. Vehicle Speed Estimation Error Analysis

Figs.13-15 compares the estimated speed and real speed in each type. In addition, the histograms of our proposed models in three types are presented to show the distribution of errors. As in Fig 16-18, the observation of the four model's estimation error distributions are clearly seen. Among all the three types of vehicles, the speed estimation in model 4 has the closest

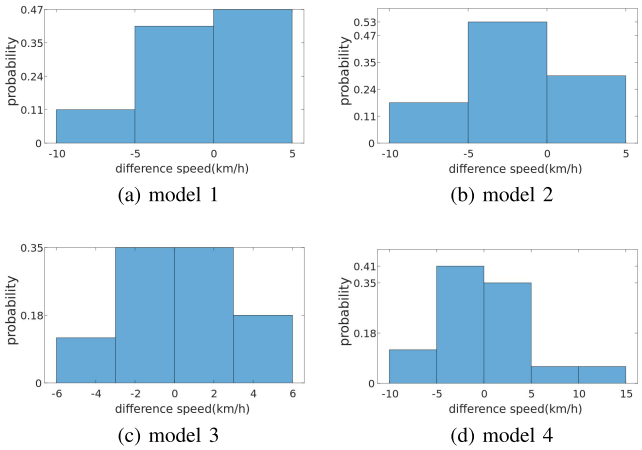

Fig. 16. Histograms for sedans.

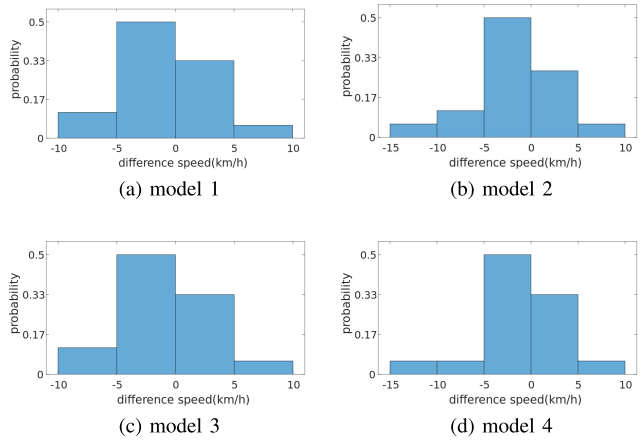

Fig. 17. Histograms for SUVs and vans.

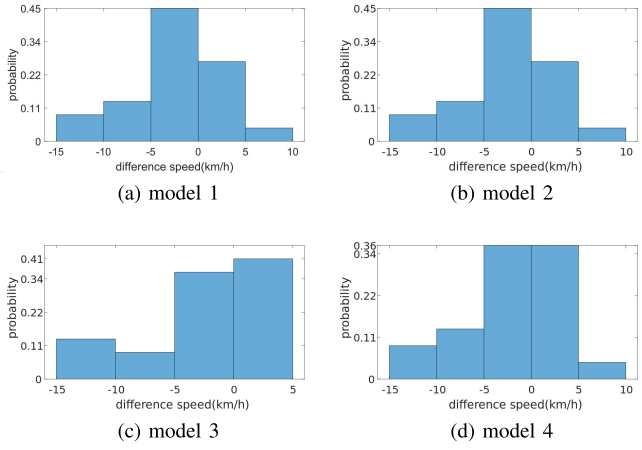

Fig. 18. Histograms for buses and trucks.

match with the theoretical analysis in (11), and it has the best performance in all models.

V. Conclusion

In this paper, we addressed the problems of driving vehicles classification and accurate vehicle speed estimation in urban environments through a magnetic sensor. In particular, we developed a vehicle classification and speed estimation technique, MagMonitor, which utilized vehicle magnetic characteristics to classify vehicle types and through normalized and filtered magnetic waveform characteristics to estimate vehicle types and speeds. Also, road experiments were conducted to validate the effectiveness of the proposed technique. The magnetic sensor in our experiment is tiny, cost-effective, and environmental-friendly. It is part of our future work to combine with other sensor information to improve the performance of the fine-grained speed estimation. We will also study vehicle classification on multiple lanes in the future.

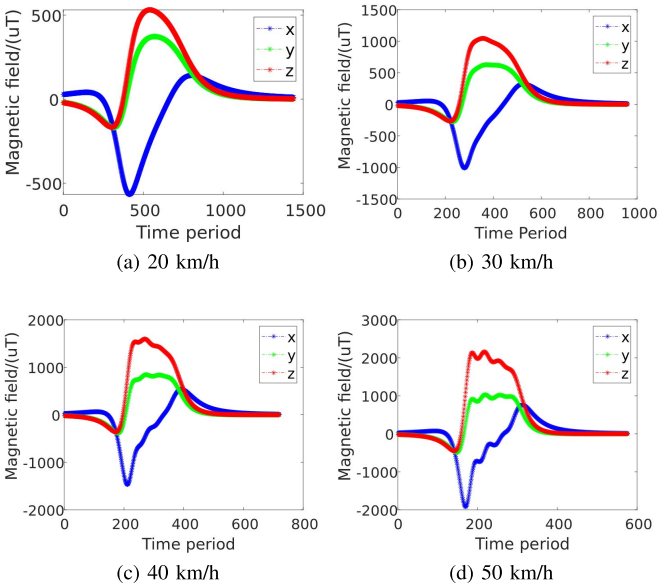

Fig. 19. For a bus with a length of 12 m, the wave perturbations in 20 km/h, 30 km/h, 40 km/h, 50 km/h speeds, respectively.

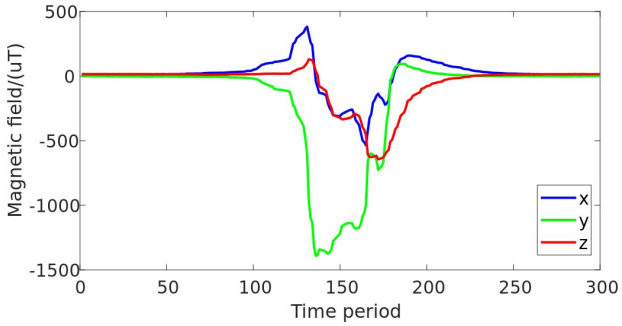

Fig. 20. The real-time magnetic perturbation caused by a bus driving in 50 km/h.

Appendix

Here, for a bus with a length of 12 m, combined with real experiment knowledge, we assume the vehicle can be modeled by four magnetic dipoles and we list the respective wave patterns for the speed varying from 20 km/h to 50 km/h. (Figs. 19 (a) - (d)).

Fig. 20 shows the magnetic perturbation caused by a bus. It is obvious to see that using four magnetic dipoles to simulate a long vehicle is reasonable.

ACKNOWLEDGMENT

The authors would like to thank the students from Xidian University for the road experiment assistance. They also would like to thank the anonymous reviewers for their comments.

REFERENCES

[1] W. Xu *et al.*, "Internet of vehicles in big data era," *IEEE/CAA J. Automatica Sinica*, vol. 5, no. 1, pp. 19–35, Jan. 2018.
[2] Y. Lv, Y. Duan, W. Kang, Z. Li, and F.-Y. Wang, "Traffic flow prediction with big data: A deep learning approach," *IEEE Trans. Intell. Transp. Syst.*, vol. 16, no. 2, pp. 865–873, Apr. 2015.
[3] K. Garg, N. Ramakrishnan, A. Prakash, and T. Srikanthan, "Rapid and robust background modeling technique for low-cost road traffic surveillance systems," *IEEE Trans. Intell. Transp. Syst.*, vol. 21, no. 5, pp. 2204–2215, May 2020.
[4] B.-L. Ye *et al.*, "A survey of model predictive control methods for traffic signal control," *IEEE/CAA J. Automatica Sinica*, vol. 6, no. 3, pp. 623–640, May 2019.
[5] M. Zhou, H. Dong, P. A. Ioannou, Y. Zhao, and F.-Y. Wang, "Guided crowd evacuation: Approaches and challenges," *IEEE/CAA J. Automatica Sinica*, vol. 6, no. 5, pp. 1081–1094, Sep. 2019.
[6] R. O. Chavez-Garcia and O. Aycard, "Multiple sensor fusion and classification for moving object detection and tracking," *IEEE Trans. Intell. Transp. Syst.*, vol. 17, no. 2, pp. 525–534, Feb. 2016.
[7] *National Center for Statistics and Analysis*, National Highway Traffic Safety Administration, Washington, DC, USA, Mar. 2018.
[8] C. Sun and S. G. Ritchie, "Individual vehicle speed estimation using single loop inductive waveforms," *J. Transp. Eng.*, vol. 125, no. 6, pp. 531–538, Nov. 1999.
[9] T. N. Schoepflin and D. J. Dailey, "Dynamic camera calibration of roadside traffic management cameras for vehicle speed estimation," *IEEE Trans. Intell. Transp. Syst.*, vol. 4, no. 2, pp. 90–98, Jun. 2003.
[10] S. Taghvaeeyan and R. Rajamani, "Portable roadside sensors for vehicle counting, classification, and speed measurement," *IEEE Trans. Intell. Transp. Syst.*, vol. 15, no. 1, pp. 73–83, Feb. 2014.
[11] Q. Wei and B. Yang, "Adaptable vehicle detection and speed estimation for changeable urban traffic with anisotropic magnetoresistive sensors," *IEEE Sensors J.*, vol. 17, no. 7, pp. 2021–2028, Apr. 2017.
[12] W. Balid, H. Tafish, and H. H. Refai, "Development of portable wireless sensor network system for real-time traffic surveillance," in *Proc. IEEE 18th Int. Conf. Intell. Transp. Syst.*, Sep. 2015, pp. 1630–1637.
[13] C. Wang, Z. Xie, L. Shao, Z. Zhang, and M. Zhou, "Estimating travel speed of a road section through sparse crowdsensing data," *IEEE Trans. Intell. Transp. Syst.*, vol. 20, no. 9, pp. 3486–3495, Sep. 2019.
[14] S.-L. Jeng, W.-H. Chieng, and H.-P. Lu, "Estimating speed using a side-looking single-radar vehicle detector," *IEEE Trans. Intell. Transp. Syst.*, vol. 15, no. 2, pp. 607–614, Apr. 2014.
[15] H. Han *et al.*, "SenSpeed: Sensing driving conditions to estimate vehicle speed in urban environments," in *Proc. IEEE INFOCOM - IEEE Conf. Comput. Commun.*, Apr. 2014, pp. 727–735.
[16] E. J. Wang, T.-J. Lee, A. Mariakakis, M. Goel, S. Gupta, and S. N. Patel, "Magnifisense: Inferring device interaction using wrist-worn passive magneto-inductive sensors," in *Proc. ACM Int. Joint Conf. Pervasive Ubiquitous Comput.*, 2015, pp. 15–26.
[17] A. Haoui, R. Kavaler, and P. Varaiya, "Wireless magnetic sensors for traffic surveillance," *Transp. Res. C, Emerg. Technol.*, vol. 16, no. 3, pp. 294–306, Jun. 2008.
[18] S. Y. Cheung, S. Coleri, B. Dundar, S. Ganesh, C.-W. Tan, and P. Varaiya, "Traffic measurement and vehicle classification with single magnetic sensor," *Transp. Res. Rec., J. Transp. Res. Board*, vol. 1917, no. 1, pp. 173–181, Jan. 2005.
[19] Q. Wang, J. Zheng, H. Xu, B. Xu, and R. Chen, "Roadside magnetic sensor system for vehicle detection in urban environments," *IEEE Trans. Intell. Transp. Syst.*, vol. 19, no. 5, pp. 1365–1374, May 2018.
[20] R. Hostettler, W. Birk, and M. L. Nordenvaad, "Feasibility of road vibrations-based vehicle property sensing," *IET Intell. Transp. Syst.*, vol. 4, no. 4, pp. 356–364, 2010.
[21] S. V. Marshall, "Vehicle detection using a magnetic field sensor," *IEEE Trans. Veh. Technol.*, vol. 27, no. 2, pp. 65–68, May 1978.
[22] W. Balid, H. Tafish, and H. H. Refai, "Intelligent vehicle counting and classification sensor for real-time traffic surveillance," *IEEE Trans. Intell. Transp. Syst.*, vol. 19, no. 6, pp. 1784–1794, Jun. 2018.
[23] D. Obertov, V. Bardov, and B. Andrievsky, "Vehicle speed estimation using roadside sensors," in *Proc. 6th Int. Congr. Ultra Modern Telecommun. Control Syst. Workshops (ICUMT)*, Oct. 2014, pp. 111–117.
[24] H. Li, H. Dong, L. Jia, D. Xu, and Y. Qin, "Some practical vehicle speed estimation methods by a single traffic magnetic sensor," in *Proc. 14th Int. IEEE Conf. Intell. Transp. Syst. (ITSC)*, Oct. 2011, pp. 1566–1573.
[25] X. Deng, Z. Hu, P. Zhang, and J. Guo, "Vehicle class composition identification based mean speed estimation algorithm using single magnetic sensor," *J. Transp. Syst. Eng. Inf. Technol.*, vol. 10, no. 5, pp. 35–39, Oct. 2010.
[26] J. Lan, Y. Xiang, L. Wang, and Y. Shi, "Vehicle detection and classification by measuring and processing magnetic signal," *Measurement*, vol. 44, no. 1, pp. 174–180, Jan. 2011.
[27] S. Y. Cheung, S. C. Ergen, and P. Varaiya, "Traffic surveillance with wireless magnetic sensors," in *Proc. 12th ITS World Congr.*, vol. 1917, 2005, p. 173181.
[28] D. Kleyko, R. Hostettler, W. Birk, and E. Osipov, "Comparison of machine learning techniques for vehicle classification using road side sensors," in *Proc. IEEE 18th Int. Conf. Intell. Transp. Syst.*, Sep. 2015, pp. 572–577.
[29] H. Liu, M. Zhou, and Q. Liu, "An embedded feature selection method for imbalanced data classification," *IEEE/CAA J. Automatica Sinica*, vol. 6, no. 3, pp. 703–715, May 2019.
[30] P. Zhang, S. Shu, and M. Zhou, "An online fault detection model and strategies based on SVM-grid in clouds," *IEEE/CAA J. Automatica Sinica*, vol. 5, no. 2, pp. 445–456, Mar. 2018.
[31] N. Wahlstrom, R. Hostettler, F. Gustafsson, and W. Birk, "Classification of driving direction in traffic surveillance using magnetometers," *IEEE Trans. Intell. Transp. Syst.*, vol. 15, no. 4, pp. 1405–1418, Aug. 2014.
[32] J. Xie *et al.*, "The simulations and experiments of the electromagnetic tracking system based on magnetic dipole model," *IEEE Trans. Appl. Supercond.*, vol. 24, no. 3, pp. 1–4, Jun. 2014.
[33] N. Wahlstrom and F. Gustafsson, "Magnetometer modeling and validation for tracking metallic targets," *IEEE Trans. Signal Process.*, vol. 62, no. 3, pp. 545–556, Feb. 2014.
[34] S. Gontarz, P. Szulim, J. Seńko, and J. Dybała, "Use of magnetic monitoring of vehicles for proactive strategy development," *Transp. Res. C, Emerg. Technol.*, vol. 52, pp. 102–115, Mar. 2015. [Online]. Available: http://www.sciencedirect.com/science/article/pii/S0968090X1400357X
[35] Q. Zhou, G. Tong, B. Li, and X. Yuan, "A practicable method for ferromagnetic object moving direction identification," *IEEE Trans. Magn.*, vol. 48, no. 8, pp. 2340–2345, Aug. 2012.
[36] S. Gontarz and S. Radkowski, "Impact of various factors on relationships between stress and eigen magnetic field in a steel specimen," *IEEE Trans. Magn.*, vol. 48, no. 3, pp. 1143–1154, Mar. 2012.
[37] Y. Ren, C. Hu, S. Xiang, and Z. Feng, "Magnetic dipole model in the near-field," in *Proc. IEEE Int. Conf. Inf. Autom.*, Aug. 2015, pp. 1085–1089.
[38] Y. Feng, G. Mao, B. Cheng, B. Huang, S. Wang, and J. Chen, "MagSpeed: A novel method of vehicle speed estimation through a single magnetic sensor," in *Proc. IEEE Intell. Transp. Syst. Conf. (ITSC)*, Oct. 2019, pp. 4281–4286.
[39] Z. Chen *et al.*, "Roadside sensor based vehicle counting incomplex traffic environment," in *Proc. IEEE Globecom Workshops (GC Wkshps)*, Dec. 2019, pp. 1–5.
[40] G. Chandrasekaran *et al.*, "Tracking vehicular speed variations by warping mobile phone signal strengths," in *Proc. IEEE Int. Conf. Pervas. Comput. Commun. (PerCom)*, Mar. 2011, pp. 213–221.

Yimeng Feng (Graduate Student Member, IEEE) received the B.S. degree from the Beijing University of Posts and Telecommunications, Beijing, China, and the Queen Mary University of London, London, U.K., in 2016. She is currently pursuing the dual Ph.D. degree program with the State Key Laboratory of Networking and Switching Technology, Beijing University of Posts and Telecommunications, and the School of Electrical and Data Engineering, University of Technology Sydney, Ultimo, NSW, Australia. Her current research interests include intelligent transportation systems, the Internet of Things, and wireless sensor network technology. She has served as a TPC member and a reviewer in a number of international conferences.

Guoqiang Mao (Fellow, IEEE) was with the University of Technology Sydney and the University of Sydney. He is currently a Distinguished Professor with Xidian University. He has published more than 200 articles in international conferences and journals, which have been cited more than 9000 times. His research interests include intelligent transport systems, applied graph theory and its applications in telecommunications, the Internet of Things, wireless sensor networks, wireless localization techniques and network modeling, and performance analysis. He is a fellow of IET. He received the Top Editor Award for outstanding contributions to the IEEE TRANSACTIONS ON VEHICULAR TECHNOLOGY in 2011, 2014, and 2015. He was the Co-Chair of the IEEE Intelligent Transport Systems Society Technical Committee on Communication Networks. He has served as the chair, the co-chair, and a TPC member in a number of international conferences. He was an Editor of the IEEE TRANSACTIONS ON WIRELESS COMMUNICATIONS from 2014 to 2019. He has been an Editor of the IEEE TRANSACTIONS ON INTELLIGENT TRANSPORTATION SYSTEMS since 2018 and the IEEE TRANSACTIONS ON VEHICULAR TECHNOLOGY since 2010.

Bo Cheng (Member, IEEE) received the Ph.D. degree in computer science and engineering from the University of Electronic Science and Technology of China, in 2006. He has been with the Beijing University of Posts and Telecommunications (BUPT) since 2008, where he is currently a Full Professor with the Research Institute of Networking Technology. His current research interests include network services and intelligence, the Internet of Things technology, and multimedia communications.

Changle Li (Senior Member, IEEE) received the Ph.D. degree in communication and information system from Xidian University, China, in 2005. He conducted his Post-Doctoral Research in Canada and the National Institute of Information and Communications Technology, Japan. He has been a Visiting Scholar with the University of Technology Sydney. He is currently a Professor with the State Key Laboratory of Integrated Services Networks, Xidian University. His research interests include intelligent transportation systems, vehicular networks, mobile ad-hoc networks, and wireless sensor networks.

Yilong Hui (Member, IEEE) received the Ph.D. degree from Shanghai University, China, in 2018. He is currently a Lecturer with the State Key Laboratory of Integrated Services Networks, Xidian University, China. His research interests are in the general area of wireless network architecture, vehicular networks, and smart city transportation.

Zhigang Xu (Member, IEEE) received the B.S. degree in automation and the M.S. and Ph.D. degrees in traffic information engineering and control from Chang'an University, China, in 2002, 2005, and 2012, respectively. He has been a Visiting Scholar with the University of California, Davis, CA, USA, since 2015. He is currently a Professor with the School of Information Engineering, and the Director of the Laboratory of Traffic information Sensing and Control, Chang'an University. His research focuses on connected and autonomous vehicles, traffic flow analysis, transportation optimization, and intelligent transportation systems. He is also a member of the IEEE ITS Society and ASCE and the Chair of CAVs Committee of World Transportation Convention.

Junliang Chen (Senior Member, IEEE) received the B.S. degree in electrical engineering from Shanghai Jiao Tong University, China, in 1955, and the Ph.D. degree in electrical engineering from the Moscow Institute of Radio Engineering, in 1961. He has been with the Beijing University of Posts and Telecommunications (BUPT) since 1955, where he is currently the Chairman and a Professor with the Research Institute of Networking and Switching Technology. His research interests are in the area of communication networks and next-generation service creation technology. He was elected as a member of the Chinese Academy of Science in 1991 and the Chinese Academy of Engineering in 1994.